Anisotropic emission in quantum-beat spectroscopy of helium excited states

M. Lucchini,[1,*] A. Ludwig,[1] T. Zimmermann,[1] L. Kasmi,[1] J. Herrmann,[1] A. Scrinzi,[2] A. S. Landsman,[1,†] L. Gallmann,[1,3] and U. Keller[1]

[1]*Department of Physics, ETH Zurich, 8093 Zürich, Switzerland*

[2]*Ludwig-Maximilians-Universität München, Fakultät für Physik, 80333 München, Germany*

[3]*Institute of Applied Physics, University of Bern, 3012 Bern, Switzerland*

(Received 16 February 2015; revised manuscript received 27 April 2015; published 10 June 2015)

We present quantum-beat spectroscopy of excited states of helium atoms populated selectively with high-order-harmonic emission below the atomic ionization potential by means of low-pass filtering of the pump radiation. The created electron wave packet is ionized by few-cycle infrared (IR) pulses leading to characteristic peaks in the photoelectron yield, which beat with a frequency proportional to the energy gap between the states involved in the two-color photoionization process. Minimizing the direct ionization by the extreme ultraviolet (XUV) radiation, we can follow the evolution of the electron wave packet also in the region of temporal pump-probe overlap. A detailed time-frequency analysis of the quantum beats and direct comparison with the solution of the time-dependent Schrödinger equation reveal the existence of quantum beats characterized by a final state of mixed parity. Finally, we show that by varying the carrier-envelope offset phase of the probe pulse, one can optically control the preferred direction of photoelectron emission and the contrast of such beats.

DOI: 10.1103/PhysRevA.91.063406 PACS number(s): 32.80.Rm, 32.80.Qk, 42.50.Md, 42.65.Ky

I. INTRODUCTION

Quantum-beat (QB) spectroscopy is a powerful tool employed in femtochemistry [1] to study the electronic and vibrational properties of atoms and molecules [2]. Here we used QB spectroscopy in combination with high-order-harmonic (HH) excitation [3] in order to study the evolution of an electron wave packet (EWP) composed of high-lying states of He. The HH radiation corresponds to attosecond pulses in time domain, which sustain a bandwidth of several electronvolts and are centered in the vacuum ultraviolet (VUV) or extreme ultraviolet (XUV) [4,5]. Attosecond QB spectroscopy may therefore be used to study broad excitation bandwidths and tightly bound energy levels that are not reachable with infrared (IR) femtosecond excitation with unprecedented time resolution [6–8].

So far, attosecond wave-packet dynamics involving such bound states has only been studied using attosecond transient absorption spectroscopy (ATAS) [9], which recently demonstrated its potential to investigate QBs in He [10] and Ne [11]. Here we show that phenomena such as nonadiabatic Stark shift [12], population of light-induced states [13], and "direct-indirect" interference of different excitation pathways [14,15] can, in principle, also be observed in the QB signal. In contrast to ATAS, however, QB spectroscopy can be used to study the angular content of the EWP. Furthermore, the energy resolution is, in principle, limited only by the natural linewidth of the excited-state levels. In this paper, we present the experimental observation of QBs in He obtained by exciting the EWP with a tailored XUV pump, situated below the He ionization potential. This renders the measurement background free and allows for a complete study of the EWP, including the region of pump-probe overlap where the evolution of the system is strongly influenced by the IR probing field [16,17]. Furthermore, measuring the electron yield as a function of the carrier-envelope offset phase (CEP) [18] of the driving pulses and comparing with the solution of the time-dependent Schrödinger equation (TDSE), we revealed the existence of QBs with mixed parity, characterized by an asymmetric emission.

The paper is organized as follows. The physical mechanisms at the basis of the two-color photoemission of He are described in Sec. II. Section III contains the description of the experiment and the results. A time-frequency analysis and the comparison with the calculations are presented in Sec. IV, while we investigate the spatial asymmetry in photoemission and the role of the CEP in Sec. V. Finally, Sec. VI contains the conclusions.

II. PHYSICAL MECHANISMS IN TWO-COLOR PHOTOEMISSION

Both direct ionization and excitation of bound EWP can be observed when using XUV pulses with a broad spectrum centered on the atomic ionization potential. In a pump-probe experiment, the probe can subsequently ionize the excited part of the EWP and give an electron yield that oscillates with the pump-probe delay. In this case, two main contributions to the modulations are expected: (i) quantum beats [19–21] and (ii) "direct-indirect" interference [22,23]. QBs arise from the interference of different ionization pathways involving two atomic states (i, j), which give the same final electron energy. If E_i and E_j are the energies of the two excited states, then the condition $E_i + n\hbar\omega = E_j + n'\hbar\omega'$ has to be satisfied. Here, n and n' are two integer numbers describing the number of absorbed photons of energy $\hbar\omega$ and $\hbar\omega'$, respectively (with ω and ω' within the spectral bandwidth of the IR pulse). A schematic of the process is presented in Fig. 1. The XUV pulse first populates the excited states of He [Fig. 1(b)], which are subsequently ionized by the IR pulse [Fig. 1(c)]. The photoionization probability as a function of delay is thus

*mlucchini@phys.ethz.ch

†Present address: Max Planck Institute for the Physics of Complex Systems, 01187 Dresden, Germany.

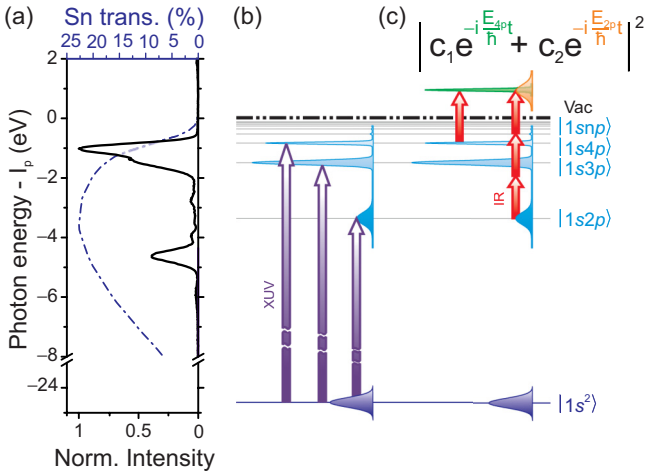

FIG. 1. (Color online) Schematic of the quantum-beating mechanism. (a) Experimental high-order-harmonic spectrum composed of only two harmonics obtained with a 200-nm-thick Sn filter. (b) Direct excitation of a coherent superposition of $1snp$ levels by absorption of XUV photons. (c) Subsequent ionization by IR photons leading, e.g., to the $4p$-$2p$ beating signal.

modulated with a frequency $\omega_{ji} = (E_j - E_i)/\hbar$ proportional to the relative energy separation of the states involved and does not depend on the final electron energy. Conversely, mechanism (ii) happens when direct XUV ionization interferes with indirect two-color ionization. The phase accumulated by the directly ionized electron depends on the final velocity. This leads to the appearance of interference fringes following hyperbolic curves [24] in the time domain or, equivalently, lines at 45° in the Fourier transform of the spectrogram.

The role of mechanisms (i) and (ii) in the photoemission from helium atoms was first investigated by Mauritsson and co-workers in Ref. [23]. The authors employed single attosecond pulses in combination with short IR pulses in a pump-probe scheme and angular detection of the photoelectron. By performing an expansion of the full angularly resolved photoelectron distribution as a sum of Legendre polynomials, they could disentangle the beating signal coming from ionization processes that end in a state of defined or mixed parity (i.e., appearing in the even or odd coefficients of the expansion). In their particular experimental configuration, the authors claim that "direct-indirect" interference is expected to involve electrons that have absorbed a different number of photons. Since an odd total number of IR photons is thus absorbed by the two interfering pathways, the signature of their interference will appear in the odd coefficients of the expansion. On the other hand, QBs were predicted to dominate in the even coefficients. As a result, this symmetry property could, in principle, be applied to isolate the QBs even if direct ionization of the target takes place. Here we show that this is not generally the case. In the presence of probe pulses characterized by a broad bandwidth, both mechanisms (i) and (ii) can indeed give final states with even or odd parity. For example, the "direct-indirect" interference between electrons directly ionized by the 17th harmonic and those which have absorbed one photon from HH15 plus two IR photons will be characterized by a final state with even parity and thus appear in the even coefficients of the expansion. Concerning mechanism (i), our results obtained without direct ionization show that QBs can as well arise from final states with mixed (odd) parity which will appear in the odd coefficients of the expansion. Furthermore, we show that the parity of the final state is strongly influenced by the probe field in the region of temporal overlap. It follows that the above-mentioned procedure cannot be applied to disentangle the contribution of mechanisms (i) and (ii) in this case.

After the first results obtained with single attosecond pulses, theoretical and experimental investigations have shown that the same kind of information can be obtained with attosecond pulse trains (APTs) [3,25,26]. Nevertheless, also in these works, direct ionization by the XUV radiation prevented a direct study of the evolution of the EWP for every value of pump-probe delay. In the next section, we will show how it is possible to tailor the pump spectrum in order to minimize the effect of mechanism (ii) and overcome this limitation.

III. EXPERIMENTAL SETUP AND RESULTS

In order to obtain a background-free measurement of QBs, we generated a comb of high-order harmonics in Xe with 15-fs IR pulses at a central wavelength of 789 nm. Details of the setup can be found in Ref. [27]. The generated HHs were subsequently filtered with a 200-nm-thick tin (Sn) foil to select only HH13 and HH15, which lie below the ionization potential of He at 24.59 eV [see Fig. 1(a)]. This procedure reduces the contrast of the APT and transforms it into a few-femtosecond XUV pulse modulated at twice the fundamental IR frequency, but

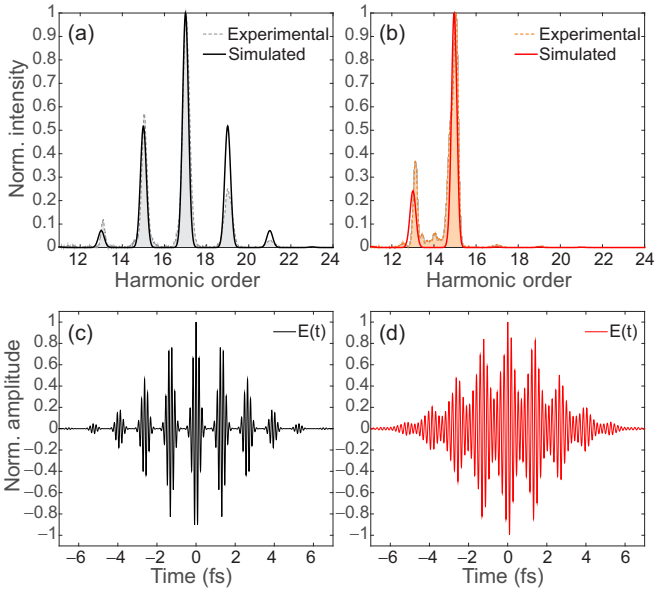

FIG. 2. (Color online) (a) Spectrum of the XUV radiation without the Sn filter. Solid line represents the simulated APT; dashed line and shaded area represent the experimental one. The simulated train has a Gaussian envelope with 5 fs FWHM. The pulses are characterized by a time duration of 400 as. (b) Same as in (a), but after filtering with the Sn foil. (c),(d) Temporal behavior of the respective simulated spectra shown in (a) and (b). As expected, the filtering procedure reduces the contrast of the individual attosecond pulses in the train, but preserves a subcycle intensity pulsation.

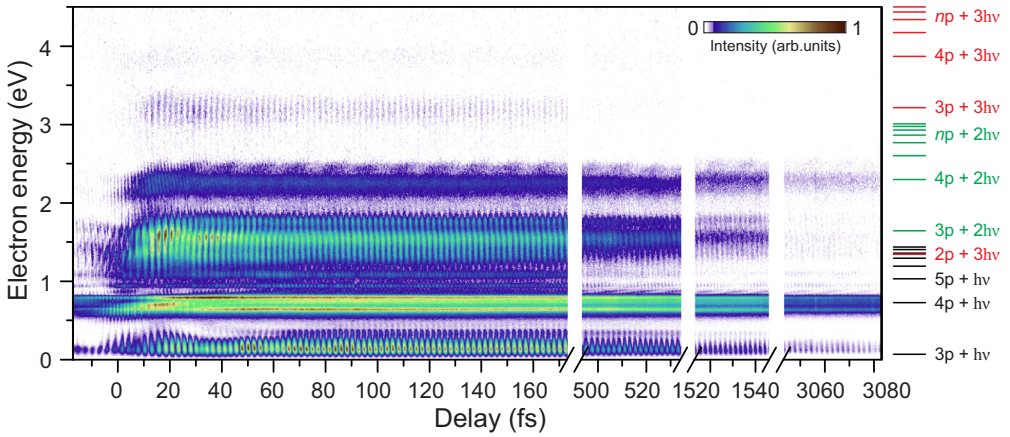

FIG. 3. (Color online) Experimental photoelectron spectra as a function of the delay between the IR femtosecond pulse and the XUV APT (positive delays correspond to XUV arriving first). Oscillations of the emission lines clearly appear in the region of pump-probe overlap and extend to positive delays. These spectral features can be attributed to two-color ionization involving one XUV photon and one to three IR photons, as underlined by the theoretical transition lines on the right. The delay axis has been calibrated by looking at the maximum electron yield in two-color ionization using the full harmonic spectrum.

still allows for subcycle resolution. Figure 2 shows the effect of the Sn filter on a numerically generated APT that resembles the experimental one. The XUV radiation was then recombined with a delayed portion of the IR pulse. Both beams were focused on a He target placed in front of a time-of-flight (TOF) spectrometer which collected the electrons emitted towards the detector in a cone with an opening angle of 30°. The IR intensity at the focus was varied between 0.9–1.5 $\times 10^{12}$ W/cm^2. The CEP of the IR pulses was actively stabilized.

Figure 3 shows the recorded photoelectron spectra as a function of the delay between the XUV and IR pulses. Each spectrum has been acquired averaging over 20 000 laser shots. A background signal with no pump was acquired every 20 delay steps. When the IR pulse arrives after XUV excitation (positive delays), peaks at the energy position of np states plus an integer number of IR photons appear. These lines correspond to a sequential two-color transition where the XUV photons first populate excited states of He and subsequently the IR ionizes them (see the horizontal lines on the right-hand side of Fig. 3). The main features appearing at 0.07, 0.73, 1.64, 2.30, 3.21, and 3.87 eV correspond to ionization of 3p and 4p states via one, two, or three IR photons, respectively. A signature of the 5p ionization appears at 1.03 eV. As the raw data already show, the signal associated with these peaks oscillates periodically with the pump-probe delay.

IV. TIME-FREQUENCY ANALYSIS AND COMPARISON WITH THEORY

A deeper understating of the atomic states forming the EWP can be obtained looking at the spectral content of the QBs. Figures 4(a) and 4(b) show the Fourier transform of the experimental data in Fig. 3 along the delay axis for the full delay range and for delays bigger than 70 fs, respectively. QBs of the 3p to 7p states with the 2p state are visible as vertical lines in both cases and are marked with blue arrows in Fig. 4(b). The total Fourier transform in Fig. 4(a) shows some additional features: first, weak tilted lines, marked with red arrows, due to the "direct-indirect" interference involving residual HH17 that is not completely suppressed by the Sn foil and, second, stronger broad features around $\hbar\omega_0 \sim 1.55$ eV predominantly positioned at the peak of the 3p state. Both features may be observed only when the pump and probe overlap in time (small delays around zero) and contain information about the behavior of the IR-dressed states, as we will discuss later on.

The time-frequency (Gabor) analysis of some selected emission lines is presented in Fig. 4(c). It shows that the QB frequencies match the unperturbed theoretical values only for long delays. For short delays, the IR field perturbs the system, polarizes the EWP, and modifies its spectral content. The strongest effect is observed in the case of the 3p-2p QB, which moves from a broad feature around $\hbar\omega_0 \simeq 1.55$ eV for short delays to its unperturbed value at 1.869 eV for long delays. A relatively strong shift may be seen also in the case of the 6p-2p QB with the unperturbed value of 2.993 eV, which is close to $2\hbar\omega_0$.

It is important to point out that in order to observe QBs with a periodicity that is noncommensurate with the frequency of the IR probe field, the starting APT (its envelope) has to be short enough. This ensures, on one side, enough bandwidth to efficiently populate the atomic state. On the other side, it minimizes the reduction in modulation contrast following the excitation of QBs by different pulses in the XUV pulse train. Figure 5 depicts a comparison of photoelectron spectra obtained with two different APTs, subsequently filtered to select only HH15 and HH13. As it is possible to observe, the use of 25-fs driving pulses instead of 15-fs pulses (first row vs second row in Fig. 5) already strongly reduces the amplitude of the QB signals. The more the beating frequency differs from $2\hbar\omega_0$, the more the QB signal is suppressed with longer excitation pulses. This can be seen in the 3p-2p QB marked by the vertical black dashed line in Figs. 5(e) and 5(f). The stronger reduction of these beats can be easily understood in terms of subsequent excitation by different pulses of the XUV radiation. During the interaction, each of the attosecond pump pulses separated in time by $T_0/2 = \pi/\omega_0$ starts a QB, which oscillates with its characteristic frequency. If this frequency is closer to ω_0, QB contributions from subsequent excitations

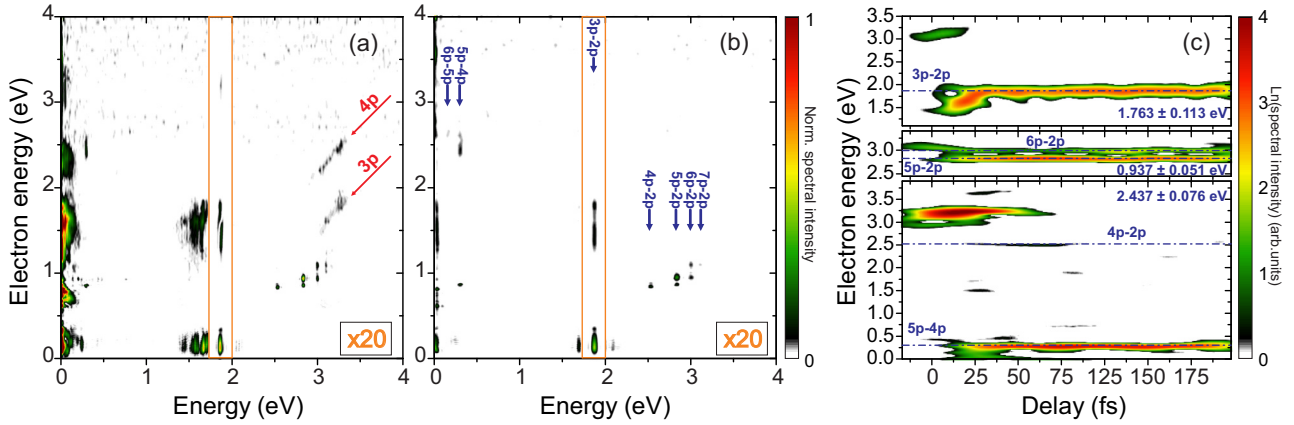

FIG. 4. (Color online) Fourier transform of the spectrogram presented in Fig. 3 along the delay axis, which allows for the identification of the states forming the EWP. (a) Total signal; (b) signal only for delays bigger than 70 fs excluding the pulse overlap region. In both cases, the spectral intensity has been multiplied by a factor of 20 outside the orange box centered around the $3p$-$2p$ QB line to better visualize the different spectral components. The QB signals involving states from $2p$ to $7p$ appear as vertical lines in both pictures. Blue arrows mark the QB energies based on the unperturbed theoretical atomic levels. In (a), the features around 3.2 eV with 45° tilt represent a signature of the direct-indirect interference. (b) These spectral features, as well as the peaks at $\hbar\omega_0 \sim 1.55$ eV, disappear for large delays. (c) A Gabor analysis of selected QBs shows how the spectral components of the EWP evolve with the delay between the pump and probe. Central energy and integration range are indicated in the three subpanels. The horizontal dot-dashed blue lines mark the theoretical position of the QBs based on an unperturbed He atom.

will be out of phase, thus giving a constant total electron yield. On the other hand, QBs which oscillate with a frequency close to twice the IR-probe frequency will be in phase and sum up constructively. Therefore, the fingerprint of the latter QBs can still be detected also with relatively long excitation XUV pulses [see Fig. 5(e)]. We want to stress that the longer the IR-probe pulses, the narrower their bandwidth and the less likely the requirement for a common final electron energy will be met. Long IR pulses may therefore reduce the strength of the QB signals independently from the pumping mechanism.

In order to confirm and interpret our observations, we solved the time-dependent Schrödinger equation (TDSE). The

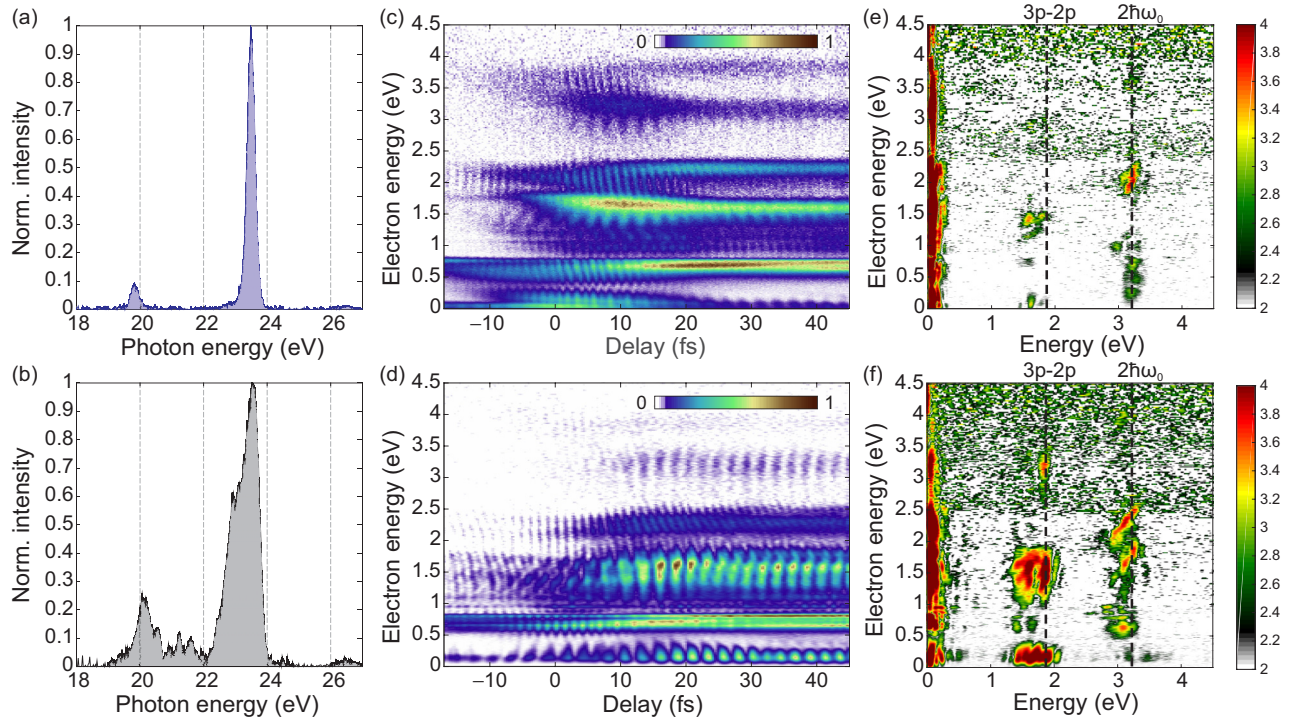

FIG. 5. (Color online) Comparison between long and short XUV excitation pulses. (a),(b) Spectra of the pump XUV pulse obtained by selecting HH15 and HH13 from an APT generated with 25-fs and 15-fs IR pulses, respectively. (c),(e) Photoelectron spectra as a function of pump-probe delay and their Fourier analysis for the XUV pump in (a) in logarithmic color scale. (d),(f) Same for the excitation pulse displayed in (b).

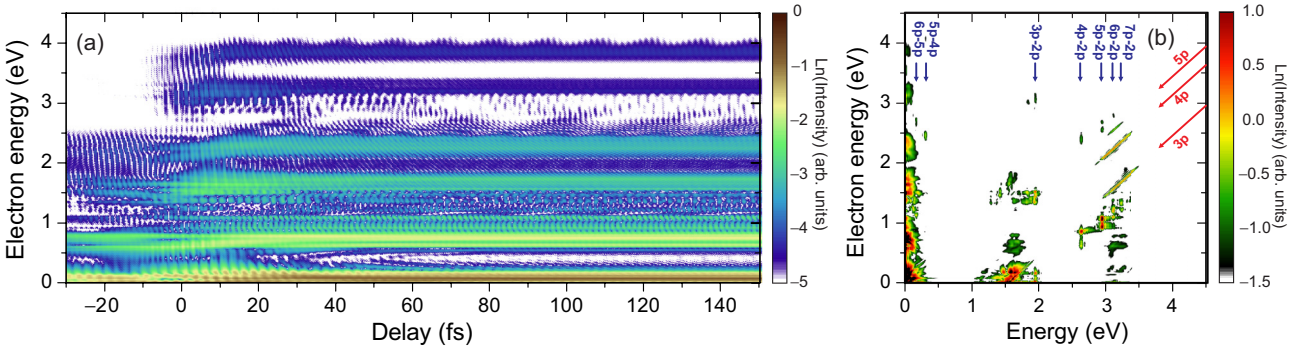

FIG. 6. (Color online) Results of the TDSE calculations. (a) Calculated spectrogram and (b) its Fourier transform. To better compare the calculated data with the experimental results, a logarithmic color map has been adopted in both. This partially compensates for the reduced collection efficiency of slow electrons in the experiment. All of the experimental features are well reproduced by the calculations.

simulations were performed using the single-electron model of He with the pseudopotential $V(r) = -(1 + \exp\{-\alpha r\})/r$, where $\alpha = 2.1325$. The solution was obtained in the velocity gauge using the adaptive-step fourth-order Runge-Kutta method with a high (12th)-order finite-element radial basis of size 192 and spherical harmonics with the degree l up to eight. Photoelectron spectra were calculated by the time-dependent surface flux (tSURFF) method [28,29] integrating the wave-function flux at the boundary of the simulation region with the diameter $R = 100$ a.u. The shapes of both pulses were taken directly from experimental measurements. The spectrum of the filtered pump consisting of only two harmonics was assumed to be equal to the experimental one in Fig. 2(b). The phase relation between the two harmonics was retrieved performing a RABBITT (Reconstruction of Attosecond Beating By Interference of Two-photon Transitions) [30] measurement with the full spectrum in Fig. 2(a) in Ar and subsequently applying the transmission of the Sn filter numerically [31]. The intensity of the filtered XUV pulse was set to 4.2×10^8 W/cm^2. The IR pulse was characterized with spectral phase interferometry for direct electric-field reconstruction (SPIDER) [32] giving a time duration of 15 fs. Its peak intensity was set to 1.72×10^{12} W/cm^2. The vector potential of both pulses was then obtained by numerical integration using the trapezoidal rule. The time step of pump-probe delays in the calculation was 0.25 fs.

The results of the numerical calculations are reported in Fig. 6. All of the major features observed experimentally are reproduced both in time domain [Fig. 6(a)] and frequency domain [Fig. 6(b)]. Furthermore, our calculations give access to the angular dependence of the electron yield in the polarization plane. In particular, they show that the $\hbar\omega_0$ signal appearing at pump-probe temporal overlap in Fig. 6(a) disappears when photoelectrons are simultaneously detected in opposite directions. This asymmetric signal, mainly detected in the $3p$-$2p$ QB, is caused by two mechanisms: different number of IR photons absorbed in the two ionization pathways and IR-induced coupling with nearby dark states. In the case of the signal corresponding to the $3p$-$2p$ QB, the electrons originating from the $2p$ state absorb one photon more than those from the $3p$ state in order to have the same final energy. As the final states of these two channels have different parity, the resulting signal depends on the direction of detection and therefore oscillates with $\hbar\omega_0$ instead of $2\hbar\omega_0$. In contrast, QBs between $2p$ and the higher-lying states ($4p$, $5p$, and $6p$), where the same final energy can be reached with the $2p$ electrons absorbing two additional IR photons, are characterized by a unique parity of the final state and thus symmetric emission. However, this simple picture can be complicated by the coupling with nearby dark states. Indeed, the coupling of the $2p$ state with the dark $3s$ and $3d$ states through the IR field can result in a nonadiabatic polarization of the excited EWP leading to an asymmetric emission, which enhances the $\hbar\omega_0$ signal. A population analysis performed projecting out the dark $3s$ and $3d$ states during the calculations shows a

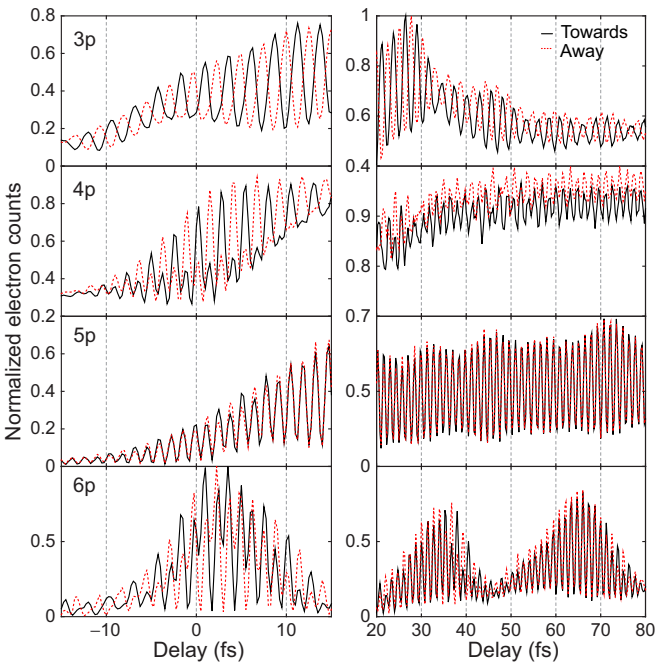

FIG. 7. (Color online) Calculated pump-probe signals for $3p$ to $6p$ ionization via one IR photon, yielding electrons at 0.21 ± 0.1, 0.68 ± 0.19, 1.02 ± 0.125, and 1.23 ± 0.05 eV. The curves represent electrons integrated in a cone with 30° opening angle. The solid black line corresponds to the cone pointing towards the detector, whereas for the red dashed line it points in the opposite direction. In contrast to the other QBs, the $3p$-$2p$ QB signals emitted in opposite directions are out of phase also for big pump-probe delays (panels on the right column).

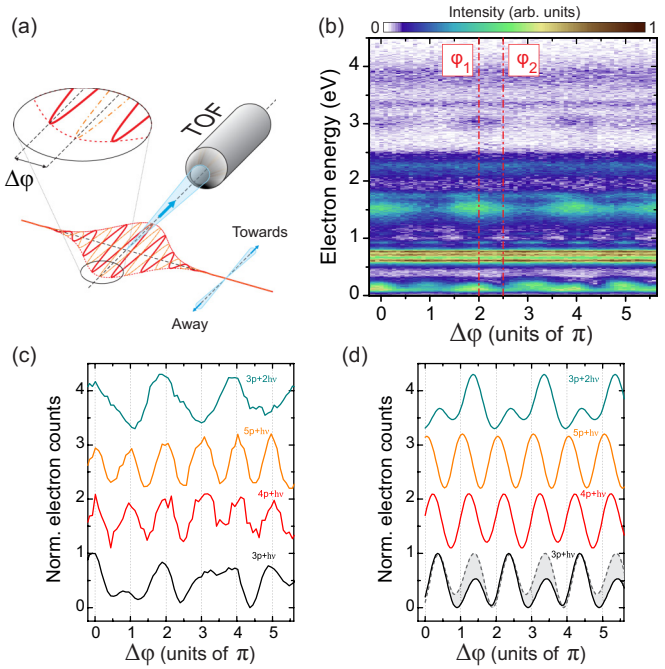

FIG. 8. (Color online) CEP dependence of the photoelectron yield at a fixed delay of 90 fs. (a) Schematic of the CEP variation inducing an effective change in the direction of detection. (b) Experimental results. (c),(d) Comparison between experiment and calculations for selected QBs. The normalized lineouts are separated by an arbitrary offset. Clear 2π periodicity is observed in the $3p$-$2p$ QB. Calculations with $3s$ and $3d$ states projected out [gray dashed line in (d)] show that the ratio between the 2π and π periodicities is strongly influenced by these states. The experimental IR intensity is $\simeq 1.5 \times 10^{12}$ W/cm^2 and 1.72×10^{12} W/cm^2 in the calculations.

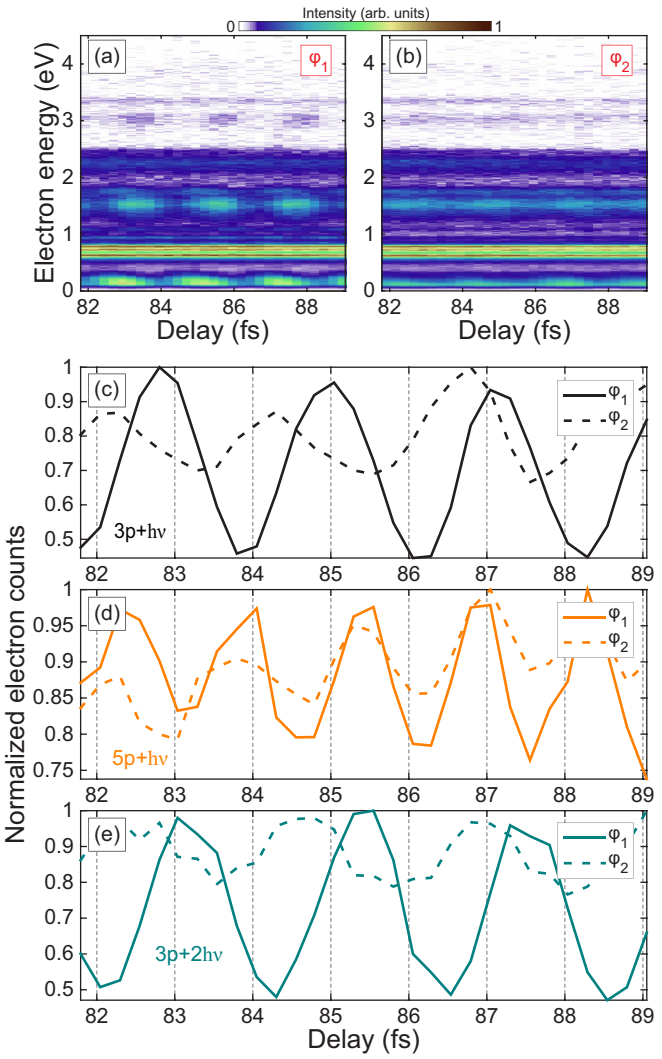

FIG. 9. (Color online) Experimental photoelectron spectra as a function of pump-probe delay and for two different values of the CEP, (a) φ_1 and (b) φ_2, marked with vertical red-dashed lines in Fig. 8(b). (c)–(e) Selected QBs corresponding to the peak in the electron yield coming from $3p + h\nu$, $5p + h\nu$, and $3p + 2h\nu$ transitions, respectively.

partial suppression of the $\hbar\omega_0$ signal corresponding to $3p$-$2p$ interference and confirms our picture. This second source of emission asymmetry can also be detected in the QBs involving the higher states even though the same number of IR photons is absorbed in this case. As it can be seen in Fig. 6, a weaker $\hbar\omega_0$ component coming from this latter mechanism, but involving the dark states $4s$ and $4d$, is present also in the emission from the $4p$ state with two IR photons. Although this signal is weak, it is still observed in the experimental data with short IR pulses [see Fig. 5(f)].

Figure 7 offers a more detailed view of the induced asymmetries. It shows a comparison between the electrons emitted in a cone with a 30° opening angle pointing either towards the detector (as in the experiment, black solid line) or in the opposite direction (red dashed line). At this point, it is convenient to make a distinction between the region of pump-probe overlap (left panels) and the region outside overlap (right panels). At the overlap, some asymmetry in the emission direction is observed for most QBs. The asymmetric signal oscillates with the laser frequency, in agreement with the previous considerations. Outside the overlap, all of the QBs besides the $3p$-$2p$ signal do not strongly depend on the detection direction. The asymmetry of the $3p$-$2p$ signal lasts even for long pump-probe delays with the frequency gradually shifting from $\hbar\omega_0$ towards the $3p$-$2p$ beating frequency as the overlap of pulses diminishes [see also Fig. 4(c)]. This demonstrates that even outside of the region of pulse overlap, the QBs can differ in parity. Performing a Legendre polynomial expansion of the photoelectron yield, the QBs corresponding to $4p$-$2p$, $5p$-$2p$, and $6p$-$2p$ will dominantly appear within the even coefficients, whereas the asymmetric $3p$-$2p$ signal will contribute mostly to the odd terms. Thus the previously proposed procedure of Legendre polynomial expansion (reported, e.g., in Ref. [23]) is unable to reliably disentangle the QB signal from the "direct-indirect" interference.

V. ROLE OF THE CEP

Although the experimental setup does not allow us to detect photoelectron spectra in opposite directions, we can probe the same effect by controlling the CEP of the generating IR field. As a CEP shift of π effectively reverses the direction of detection, we expect the amplitude of the $3p$-$2p$ QB to

modulate with 2π periodicity outside of the pump-probe overlap, while the other QBs should be π periodic. The experimental results reported in Fig. 8 confirm this picture. In addition, the calculations reveal that the nonadiabatic polarization of the EWP is important also for long delays and that the 2π-periodic component of $3p$-$2p$ QB is strongly enhanced by the presence of both $3s$ and $3d$ states.

By changing the CEP of the driving field, it is also possible to change the position of the attosecond pulses under the envelope of an APT and generate a cosinelike or a sinelike train. As discussed in Sec. IV, since the periodicity of the QBs is generally not a multiple of the IR cycle, one will expect the observed modulation contrast to strongly depend on the shape of the pump pulse train below the envelope. In order to observe this effect, we performed a delay scan for two values of the CEP differing by $\pi/2$. The values of the CEP correspond to a maximum, φ_1, and a minimum, φ_2, of the $5p$ yield and are marked by the vertical red dashed lines in Fig. 8(b). The results are presented in the spectrograms shown in Figs. 9(a) and 9(b). As one can observe, the contrast of the QBs changes strongly with the value of the CEP in a nonuniform way. The QBs which display a strong asymmetric emission [e.g., the $3p$-$2p$ QB in Figs. 9(c) and 9(e)] are more affected by the shape of the pump pulse, while the signals of the other QBs [e.g., $5p$-$2p$ in Fig. 9(d)] change less. Furthermore, for QBs characterized by a final state of mixed parity, a change in the CEP produces not only a change in the modulation contrast, but also in the timing of the oscillations. This latter effect counteracts the rotation of the IR-probe field caused by a change in the CEP.

VI. CONCLUSIONS

In conclusion, our results demonstrate that proper tailoring of the harmonic spectrum associated with an APT allows for selective excitation of electronic states, thereby excluding direct ionization. This paves the way for a detailed, background-free study of the EWP evolution in the time window where pump and probe overlap. During this time window, the dynamics of the formed EWP is deeply modified by the intense IR field, which mixes the angular components of the electronic wave function. Our results show that not all of the QBs are characterized by final states of the same parity. In these particular cases, one can control not only the amplitude of the QBs by varying the pump-probe delay, but also the preferred direction of photoelectron emission. Comparison with the solution of the TDSE shows that the IR field strongly influences the angular properties of the EWP even when pump and probe do not overlap in time. Finally, the high photon energies of the high-order harmonics make this technique suitable to study states with binding energies not accessible with IR pulses, e.g., metastable states of molecular dications. Furthermore, the combination of HH excitation with a tunable pump should pave the way for quantum-carpet spectroscopy [33] with attosecond and picometer resolution.

ACKNOWLEDGMENTS

This research was supported by the NCCR MUST, funded by the Swiss National Science Foundation and an ETH Zurich postdoctoral fellowship.

[1] A. H. Zewail, J. Phys. Chem. A **104**, 5660 (2000).
[2] R. T. Carter and J. Robert Huber, Chem. Soc. Rev. **29**, 305 (2000).
[3] N. Shivaram, H. Timmers, X.-M. Tong, and A. Sandhu, in *Frontiers in Optics 2014* (Optical Society of America, Washington, DC, 2014), p. LW5H.4.
[4] M. Ferray, A. L'Huillier, X. F. Li, L. A. Lompre, G. Mainfray, and C. Manus, J. Phys. B: At. Mol. Opt. Phys. **21**, L31 (1988).
[5] A. L'Huillier, K. J. Schafer, and K. C. Kulander, Phys. Rev. Lett. **66**, 2200 (1991).
[6] F. Krausz and M. Ivanov, Rev. Mod. Phys. **81**, 163 (2009).
[7] G. Sansone, L. Poletto, and M. Nisoli, Nat. Photon. **5**, 655 (2011).
[8] L. Gallmann, C. Cirelli, and U. Keller, Annu. Rev. Phys. Chem. **63**, 447 (2012).
[9] L. Gallmann, J. Herrmann, R. Locher, M. Sabbar, A. Ludwig, M. Lucchini, and U. Keller, Mol. Phys. **111**, 2243 (2013).
[10] M. Chini, X. Wang, Y. Cheng, and Z. Chang, J. Phys. B **47**, 124009 (2014).
[11] A. R. Beck, B. Bernhardt, E. R. Warrick, M. Wu, S. Chen, M. B. Gaarde, K. J. Schafer, D. M. Neumark, and S. R. Leone, New J. Phys. **16**, 113016 (2014).
[12] M. Chini, B. Zhao, H. Wang, Y. Cheng, S. X. Hu, and Z. Chang, Phys. Rev. Lett. **109**, 073601 (2012).
[13] S. Chen, M. J. Bell, A. R. Beck, H. Mashiko, M. Wu, A. N. Pfeiffer, M. B. Gaarde, D. M. Neumark, S. R. Leone, and K. J. Schafer, Phys. Rev. A **86**, 063408 (2012).
[14] M. Chini, X. Wang, Y. Cheng, Y. Wu, D. Zhao, D. A. Telnov, S.-I. Chu, and Z. Chang, Sci. Rep. **3**, 1105 (2013).
[15] M. Lucchini, J. Herrmann, A. Ludwig, R. Locher, M. Sabbar, L. Gallmann, and U. Keller, New J. Phys. **15**, 103010 (2013).
[16] P. Ranitovic, X. M. Tong, C. W. Hogle, X. Zhou, Y. Liu, N. Toshima, M. M. Murnane, and H. C. Kapteyn, Phys. Rev. Lett. **106**, 193008 (2011).
[17] P. Ranitovic, X. M. Tong, B. Gramkow, S. De, B. DePaola, K. P. Singh, W. Cao, M. Magrakvelidze, D. Ray, I. Bocharova, H. Mashiko, A. Sandhu, E. Gagnon, M. M. Murnane, H. Kapteyn, I. Litvinyuk, and C. L. Cocke, New J. Phys. **12**, 013008 (2010).
[18] H. Telle, G. Steinmeyer, A. Dunlop, J. Stenger, D. Sutter, and U. Keller, Appl. Phys. B **69**, 327 (1999).
[19] E. Jaynes, in *Foundations of Radiation Theory and Quantum Electrodynamics*, edited by A. Barut (Springer, New York, 1980), pp. 37–43.
[20] J. A. Yeazell and C. R. Stroud Jr., Phys. Rev. Lett. **60**, 1494 (1988).
[21] A. ten Wolde, L. D. Noordam, A. Lagendijk, and H. B. van Linden van den Heuvell, Phys. Rev. Lett. **61**, 2099 (1988).
[22] M. Wollenhaupt, A. Assion, D. Liese, C. Sarpe-Tudoran, T. Baumert, S. Zamith, M. A. Bouchene, B. Girard, A. Flettner, U. Weichmann, and G. Gerber, Phys. Rev. Lett. **89**, 173001 (2002).
[23] J. Mauritsson, T. Remetter, M. Swoboda, K. Klünder, A. L'Huillier, K. J. Schafer, O. Ghafur, F. Kelkensberg, W. Siu, P. Johnsson, M. J. J. Vrakking, I. Znakovskaya, T. Uphues, S. Zherebtsov, M. F. Kling, F. Lépine, E. Benedetti, F. Ferrari, G. Sansone, and M. Nisoli, Phys. Rev. Lett. **105**, 053001 (2010).

[24] K. Klünder, P. Johnsson, M. Swoboda, A. L'Huillier, G. Sansone, M. Nisoli, M. J. J. Vrakking, K. J. Schafer, and J. Mauritsson, Phys. Rev. A **88**, 033404 (2013).
[25] N. N. Choi, T. F. Jiang, T. Morishita, M.-H. Lee, and C. D. Lin, Phys. Rev. A **82**, 013409 (2010).
[26] H. Geiseler, H. Rottke, G. Steinmeyer, and W. Sandner, Phys. Rev. A **84**, 033424 (2011).
[27] R. Locher, M. Lucchini, J. Herrmann, M. Sabbar, M. Weger, A. Ludwig, L. Castiglioni, M. Greif, M. Hengsberger, L. Gallmann, and U. Keller, Rev. Sci. Instrum. **85**, 013113 (2014).
[28] L. Tao and A. Scrinzi, New J. Phys. **14**, 013021 (2012).
[29] V. Majety, A. Zielinski, A. Swoboda, and A. Scrinzi, The tRecX PDE solver (unpublished).
[30] H. Muller, Appl. Phys. B **74**, s17 (2002).
[31] B. Henke, E. Gullikson, and J. Davis, At. Data Nucl. Data Tables **54**, 181 (1993).
[32] C. Iaconis and I. Walmsley, Opt. Lett. **23**, 792 (1998).
[33] H. Katsuki, H. Chiba, C. Meier, B. Girard, and K. Ohmori, Phys. Chem. Chem. Phys. **12**, 5189 (2010).